Large amplitude free flexural vibrations of functionally graded graphene platelets reinforced porous composite curved beams using finite element based on trigonometric shear deformation theory

Aditya Narayan D., Tarak Ben Zineb, O. Polit, Pradyumna B., Ganapathi M.

Large amplitude free flexural vibrations of functionally graded graphene platelets reinforced porous composite curved beams using finite element based on trigonometric shear deformation theory

D. Aditya Narayan[a], T. Ben Zineb[b], O. Polit[c*], B. Pradyumna[a], M. Ganapathi[a],

Running Title: **Large amplitude vibration of porous graphene reinforced curved beams**

Acknowledgment

The authors did not receive support from any funding agencies and also confirm that they are not in any form of conflict of interest.

* Correspondence
E-mail: olivier.polit@parisnanterre.fr (O. Polit).

Highlights

- Provided the frequency-amplitude relation for porous GPL reinforced curved beams.
- Brought out the effect of distribution patterns for the pores and GPLs of beam on the nonlinear frequency.
- Presented the solution varying slenderness ratio of beams and different boundary conditions.
- Observed change in degree of hardening nonlinearity depending on the inclusion of porosity and GPL reinforcement.
- Included new results for benchmarking the solutions from other numerical approach.

Large amplitude free flexural vibrations of functionally graded graphene platelets reinforced porous composite curved beams using finite element based on trigonometric shear deformation theory

D. Aditya Narayan[a], T. Ben Zineb[b], O. Polit[c*], B. Pradyumna[a], M. Ganapathi[a]

[a]*School of Mechanical Engineering, Vellore Institute of Technology, Vellore, 632 014, India*
[b]*Université de Lorraine, CNRS, Arts et Métiers ParisTech, LEM3, F-54000 Nancy, France*
[c]*LEME, UPL, Univ. Paris Nanterre, 50 rue de Sevres, 92410, Ville d'Avray, France*

Abstract

In this paper, the large amplitude free flexural vibration characteristics of fairly thick and thin functionally graded graphene platelets reinforced porous curved composite beams are investigated using finite element approach. The formulation includes the influence of shear deformation which is represented through trigonometric function and it accounts for in-plane and rotary inertia effects. The geometric non-linearity introducing von Karman's assumptions is considered. The non-linear governing equations obtained based on Lagrange's equations of motion are solved employing the direct iteration technique. The variation of non-linear frequency with amplitudes is brought out considering different parameters such as slenderness ratio of the beam, curved beam included angle, distribution pattern of porosity and graphene platelets, graphene platelet geometry and boundary conditions. The present study reveals the redistribution of vibrating mode shape at certain amplitude of vibration depending on geometric and material parameters of the curved composite beam. Also, the degree of hardening behaviour increases with the weight fraction and aspect ratio of graphene platelet. The rate of change of nonlinear behaviour depends on the level of amplitude of vibration, shallowness and slenderness ratio of the curved beam.

Keywords: Porous curved beam; Graphene reinforcement; Nonlinear vibration; Finite element, Nonlinear Frequency; Amplitude

*Correspondence

E-mail: olivier.polit@parisnanterre.fr (O. Polit).

1. Introduction

The use of advanced materials is necessitated in aerospace technology due to the requirements of high stiffness-to and strength-to-weight ratios. Furthermore, the progress in material science along with the processing technology has led to the increased usage of porous metals and metallic foams for various applications [1-4]. The properties of such materials can be significantly improved with the addition of nano-fillers in the form of carbon nanotubes (CNTs) and graphene platelets (GPLs). The inclusion of nano-fillers effects the change in the global properties of these metallic structures depending on the weight fraction and distribution of fillers [5-7]. The structural members like beams, plates and shells made of reinforced porous materials or foams can form the integral part of various structural systems in aerospace engineering. These structural members, when subjected to supersonic flow, can experience large amplitude of vibration leading to catastrophic failure. Hence, the investigation of such porous structural members under dynamic situation continues to attract researchers for the design of reliable aerospace structural systems. Since the proposed study is related to the curved beams, the brief discussion on available studies in the literature on the large amplitudes of vibration is here restricted to beams.

The nonlinear vibration of isotropic straight beams has been studied in the past [8-15] based on various formulations such as Lagrangian-type [8] and Ritz formulation [9]. Ref. [11] brought out the approximation and assumption involved in various formulations and solution methodologies. Rao *et al.* [13] studied the non-linear vibration of beams using an eigenvalue approach by reducing the non-linear strain-displacement relations to an appropriate linear algebraic problem. Patel *et al.* [14] investigated the nonlinear free vibration of cantilever beams and brought out the in-plane inertia effect on the nonlinear behaviour and the change in mode shape with amplitudes. Pagani *et al.* [15] recently highlighted the change in nonlinear behaviour and mode change in the large deflection and post-buckling of thin-walled beams. The increased use of advanced composite materials has also recently motivated the researchers to investigate the nonlinear dynamic behaviour of laminated composite structures. Kapania and Raciti [16] analysed the free vibration of unsymmetrical laminated composite beams while Iu *et al*. [17] carried out the nonlinear forced vibration of beams taking into

consideration of damping effects. Singh *et al.* [18] extended the scope of the work presented in [16] considering higher-order theories. Here, the governing equations were obtained assuming the mode shapes and solved utilizing a direct numerical integration approach. Bassiouni *et al.*[19] examined the dynamic response of laminated composite beams through the experimental study and theoretical approach ensuring the displacement compatibility between laminas. A detailed review of available work on the vibration of composite beams was documented by Hajianmaleki and Qatu [20]. The investigation concerning dynamic characteristics of functionally graded material (FGM) beams has been carried out with great interest in recent years. Ke *et al.* [21] analysed the large amplitude vibration behaviour of Euler-Bernoulli laminated composite beams employing the Galerkin procedure and a direct numerical integration scheme coupled with the Runge-Kutta iterative method. The effect of material distributions on such behaviour was also highlighted. Kitipornchai *et al.* [22] presented a parametric study on the non-linear dynamic behaviour of cracked FGM Timoshenko beams accounting transverse shear and inertia effects. The governing equations were derived using the Ritz method in conjunction with the direct iterative method in obtaining the non-linear frequencies. Wu *et al*. [23] described the non-linear vibration of functionally graded carbon nanotube (FG-CNT) reinforced beams and their sensitivity analysis considering geometric imperfections based on the formulation outlined in [22]. Feng *et al.* [24] attempted the large amplitude vibration behaviour of Timoshenko FGM beams reinforced with graphene platelets. The governing differential equations, obtained using Hamilton's principle, were solved analytically employing the Ritz method coupled with the direct iteration technique. It may be noted in this discussion that all these studies are concerned with the straight beam analysis.

Few notable contributions to the study of isotropic curved beams or shallow arches in the past discussed in Refs. [25-28]. In Ref. [25], a modified modal equation for curved beams based on the Duffing equation was formulated and the solution was obtained by integration using a fourth order Runge-Kutta method. A mixed type finite element approach using Reissner-type variational statement was proposed in Ref. [26] whereas an analytical formulation introducing Lagrangian variational method was employed in [27]. A shear flexible field consistent curve beam element based on a spline

function was examined for the nonlinear dynamic analysis of curved beams in [28]. Ganapathi *et al.* [29] studied the large amplitude vibrations of laminated composite curved beams extending the element proposed in [28] and proposing the Newton-Raphson iterative method to achieve the required convergence. They concluded that the type of nonlinearity can alter with respect to amplitude of vibration and geometric parameter of curved beam. At higher amplitude of vibration, the occurrence of redistribution of mode shape and the possibility of higher modes are reported. Hajianmaleki and Qatu [30] developed a general approach for studying the vibration of curved beams by implementing curvature terms in the strain-displacement equations. It may be opined, to the best of authors' knowledge, there is no study reported in literature on the large amplitude vibrations of functionally graded graphene or CNT reinforced curved beams.

In the present work, the non-linear free flexural vibration of functionally graded graphene platelets reinforced porous composite beams is investigated based on a trigonometric refined model as described by Touratier [31] and Ganapathi *et al.* [32]. The governing equations developed are solved using a direct iteration method. The formulation developed here is validated against the available work in the literature. A detailed numerical study is carried out considering various parameters such as the effect of slenderness ratio of the beam, curved beam included angle, distribution pattern of porosity and graphene platelets, and boundary conditions on the frequency–amplitude relationship.

The paper is structured as follows: the material aspects of graded porosity distribution and GPL patterns are shown in section 2, followed by describing the curved beam theory and governing equations in section 3. The solution methodology is briefly highlighted in Section 4. Section 5 comprises the assessment of the formulation and the detailed numerical studies followed by the conclusion.

2. Formulation of effective properties

The material considered here is a porous curved beam involving metal foam which is reinforced with graphene nano-platelets. The porosity is presumed as closed-cells in nature and is distributed through the thickness in different patterns. The graphene platelet properties are governed by their geometric parameters and are also distributed through the thickness in different forms. The evaluation of the effective properties is briefly outlined here [33-38].

2.1. Distribution of porosity

The material properties of a closed cell porous structure are presumed to change in the thickness plane as a function of z coordinate as indicated in Fig. 1. The effective mass density and Young's modulus are written as follows [39-41]

$$\rho(z) = \hat{\rho}[1 - e_m\lambda(z)]$$

$$E(z) = \hat{E}\left[1 - e_p\lambda(z)\right] \tag{1}$$

where $\hat{\rho}$ & $\hat{E}$ are the density and Young's modulus of nanocomposite curved beam, respectively, without having any defects like pores/porosity; e_m & e_p are porosity coefficients pertaining to density and stiffness functions, respectively. $\lambda(z)$ refers three porosity dispersion patterns that are selected here as uniform, symmetric and unsymmetric variations [24], as represented in Fig. 1a and is shown below as

$$\lambda(z) = \begin{cases} \lambda_0 \\ \cos\left(\frac{\pi z}{h}\right) \\ cos\left(\frac{\pi z}{2h} + \pi/4\right) \end{cases} \tag{2}$$

The coefficient e_p related to the stiffness function given in Eq. (1) is treated as

$$e_p = 1 - \bar{E}_2/\bar{E}_1 \tag{3}$$

where $\bar{E}_1$ & $\bar{E}_2$ are the high and low values of Young's moduli of GPL reinforced curved beams with the presence of non-uniform porous dispersion, respectively. The constant e_p is considered to be one of the primary parameters for the design of such structures.

The relationship between the porosity coefficients e_p and e_m involved in Eq. (1) can be obtained using the curve fitting equation developed for ($E(z)/\hat{E}$) from the data generated by Gaussian Random Field model [42,43] as

$$e_m = \frac{1.121\left[1-\left(1-e_p\lambda(z)\right)^{\frac{1}{2.3}}\right]}{\lambda(z)} \tag{4}$$

Similarly, the fitting data formed for the effective Poisson's ratio [38(39)] is given as

$$\nu(z) = 0.221e_m\lambda(z) + \hat{\nu}(0.342\,[e_m\lambda(z)]^2 - 1.21e_m\lambda(z) + 1) \tag{5}$$

To compute the λ_0 value of the uniform porosity distribution case, Eq. (2), it is assumed that the total weight of the beam is constant, irrespective of the variation in the porosity distribution. This allows one to find the value of λ_0 using a reference distribution such as the symmetric case, and by using Eq. (4) in the density equation Eq. (1) as

$$\lambda_o = \frac{1}{e_p}\left[1 - \left(\frac{1/h\int_{-h/2}^{h/2}\rho(z)/\hat{\rho}\,dz + 0.121}{1.121}\right)^{2.3}\right] \tag{6}$$

With the above details, the equivalent material properties of the GPL reinforced matrix, considering the introduction of porosity in a GPL reinforced composite, can be found. To evaluate this, the beam can be first considered to be reinforced with GPLs, thus forming as pure nano-composites. The elastic modulus $\hat{E}$ of such beam is estimated from the expression of the Halpin-Tsai data model [33(35)] while the density $\hat{\rho}$ and Poisson's ratio $\hat{\nu}$ for the same case are found by using rule of mixtures as shown below.

$$\hat{E} = \frac{3}{8}\left(\frac{1+\alpha_{gpl}^{l}\beta_{gpl}^{l}V_{gpl}}{1-\beta_{gpl}^{l}V_{gpl}}\right)E_m + \frac{5}{8}\left(\frac{1+\alpha_{gpl}^{w}\beta_{gpl}^{w}V_{gpl}}{1-\beta_{gpl}^{l}V_{gpl}}\right)E_m \tag{7}$$

$$\hat{\rho} = \rho_{gpl}V_{gpl} + \rho_m V_m \tag{8}$$

$$\hat{\nu} = \nu_{gpl}V_{gpl} + \nu_m V_m \tag{9}$$

where $V_m = 1 - V_{gpl}$.

The material parameters V_{gpl} & V_m, respectively, denote the volume fractions of GPLs and matrix material presented in the resultant composite, respectively; ν_{gpl}& ν_m , ρ_{gpl}&ρ_m are the mass densities, Poisson's ratios of GPLs and matrix, respectively; E_m is the elastic modulus of the matrix.

The geometry parameters of graphene platelet ($\alpha_{gpl}^{l}, \alpha_{gpl}^{w}$) can be written in terms of GPL thickness and aspect ratios; β_{gpl}^{l}, β_{gpl}^{w} are related to the elastic modulus ratio of GPL and matrix, and GPL geometric parameters, respectively as

$$\alpha_{gpl}^{l} = \frac{2l_{gpl}}{t_{gpl}} \; ; \; \alpha_{gpl}^{w} = \frac{2w_{gpl}}{t_{gpl}} \tag{10a}$$

$$\beta_{gpl}^{l} = \frac{(E_{gpl}/E_m)-1}{(E_{gpl}/E_m)-\alpha_{gpl}^{l}} \; ; \; \beta_{gpl}^{w} = \frac{(E_{gpl}/E_m)-1}{(E_{gpl}/E_m)+\alpha_{gpl}^{w}} \tag{10b}$$

Here, t_{gpl}, w_{gpl} & l_{gpl} are the GPL thickness, breath, and length, respectively; E_{gpl} is the elatistic modulus of the GPL fillers.

2.2. GPL distribution

The volume fraction V_{gpl} in Eq. (11) is changed in the thickness direction assuming various dispersion forms (uniform, symmetric and unsymmetrical cases) as shown in Fig. 1b and can be stated as

$$V_{gpl} = \begin{cases} V_1^j \\ V_2^j[1-\cos(\pi z/h)] \\ V_3^j\left[1-\cos\left(\frac{\pi z}{2h}+\pi/4\right)\right] \end{cases} \tag{11}$$

where the superscript *j* indicates the dispersion pattern of porosity.

The volume fraction V_{gpl}, in general, can be linked with the GPL weight fraction (W_{gpl}) as

$$V_{gpl} = \frac{W_{gpl}}{W_{gpl}+\rho_{gpl}/\rho_M(1-W_{gpl})} \tag{12}$$

The maximum value V_i in Eq. (11) can be computed using Eqs. (11), (12) in conjunction with the relative weights calculated from Eq. (1) for the selected porosity and GPL distributions as

$$\int_{-h/2}^{h/2} V_{gpl}\ [1-e_m\ \lambda(z)]\ dz\ = \frac{W_{gpl}}{[W_{gpl}+(\rho_{gpl}/\rho_m)\ (1-W_{gpl})]} \int_{-h/2}^{h/2} [1-e_m\ \lambda(z)]\ \ dz \tag{13}$$

3. Structural formulation and solution methodology

The curved beam model considered here is defined by length *L*, thickness *h*, unit width, and radius of curvature *R* having beam included angle ϕ, as illustrated in Fig. 2a. The structural behavior is defined following a trigonometric shear deformation theory that utilizes a sinusoidal function in

representing the deformation of the beam cross-section, referred as the SIN model [30,33,44]. The displacements in the x direction along the length and $z\,\epsilon(-\frac{h}{2},\frac{h}{2})$ direction i.e the thickness direction, are represented by u and w respectively and are related to the field variables as follows

$$\begin{cases} u_1(x,z,t) = \left(1+\frac{z}{R}\right)u_0(x,t) - z\,w'_0(x,t) + \Gamma(z)\,\gamma_0(x,t) \\ u_3(x,z,t) = w_0(x,t) \end{cases} \tag{14}$$

where t is the time, and the transverse shear strain contribution γ_0 can be given as

$$\gamma_0(x,t) = \theta(x,t) + w'_0(x,t) - \frac{1}{R}u_0(x,t) \tag{15}$$

The kinematics assumed here has three field variables as functions of x and t; u_0 is the curvilinear axial displacement; w_0 is the transverse displacement along the beam neural axis; θ is the rotation of the cross-section. Derivatives are denoted by $(\ )' = \partial/\partial x$ and $(\dot{}) = \partial/\partial t$. The function $\Gamma(z)$ in Eq. (14) is used to deduce different theories, for instance, the classical Euler Bernoulli theory by $\Gamma(z) = 0$, Timoshenko theory by $\Gamma(z) = z$, and or the SIN theory by $\Gamma(z) = \frac{h}{\pi}\sin\frac{\pi z}{h}$.

The strains obtained from the kinematic equations including von-Karman's assumptions are stated as follows

$$\{\varepsilon\} = \{\varepsilon_L\} + \{\varepsilon_{NL}\} \tag{16a}$$

which can be further expanded as:

$$\begin{Bmatrix} \varepsilon_{11} \\ \gamma_{13} \end{Bmatrix} = \begin{Bmatrix} u'_0 + \frac{w_0}{R} + z\left(\frac{u'_0}{R} - w''_0\right) + \Gamma(z)\gamma'_0 \\ \Gamma'(z)\gamma'_0 \end{Bmatrix} + \begin{Bmatrix} \frac{1}{2}(w'_0)^2 \\ 0 \end{Bmatrix} \tag{16b}$$

and the relation between these strains with stresses by the constitutive law are

$$\begin{Bmatrix} \sigma_{11} \\ \sigma_{13} \end{Bmatrix} = \begin{Bmatrix} C_{11}\varepsilon_{11} \\ C_{66}\,\gamma_{13} \end{Bmatrix} \tag{17}$$

where $C_{11} = \frac{E}{1-\nu^2}$; $\quad C_{66} = G$

For the material model considered here, the shear modulus G can be connected to the Young's modulus E by $E = 2G(1+\nu)$.

The equations of motion are in general developed through the Lagrangian equations of motion by

$$\frac{\mathrm{d}}{\mathrm{dt}}\left[\frac{\partial(T-U)}{\partial\dot{\delta}_{\mathrm{i}}}\right]-\left[\frac{\partial(T-U)}{\partial\delta_{\mathrm{i}}}\right]=0, i=1,2,\ldots n \tag{18}$$

where, δ_{i} is the vector of global degrees of freedom; U is the strain energy, T is the kinetic energy. All these energy contributions can be expressed as

$$U_s(\delta_{\mathrm{i}})=\int_0^L\int_{-\frac{h}{2}}^{\frac{h}{2}}(\varepsilon^T\sigma)dzdx=\frac{1}{2}\{\delta\}^T\left[[K_L]+\frac{1}{3}[K_{NL1}(\delta)]+\frac{1}{6}[K_{NL2}(\delta)]\right]\{\delta\}\ ; \tag{19a}$$

$$T(\delta_{\mathrm{i}})=\frac{1}{2}\int_0^L\int_{-\frac{h}{2}}^{\frac{h}{2}}\rho(\dot{u}_1{}^2+\dot{u}_3{}^2)\,dx\,dz \tag{19b}$$

where $[K_L]$ is the linear global stiffness matrix; $[K_{NL1}]$ and $[K_{NL2}]$ comprise the non-linear stiffness matrices that are linearly and quadratically dependent on the field variables, respectively.

Substituting Eq. (19) in Lagrange's equation of motion (18), the governing equations for the nonlinear free vibration of beams is obtained as

$$[M]\{\ddot{\delta}\}+\left[[K_L]+\frac{1}{2}[K_{NL1}]+\frac{1}{3}[K_{NL2}]\right]\{\delta\}=0 \tag{20}$$

Here, [M] is the consistent mass matrix of the beam.

Substituting characteristics of the time function at the point of reversal of motion

$$\{\ddot{\delta}\}=-\omega^2\{\delta\} \tag{21}$$

Equation (20) will lead to the following non-linear algebraic equation form:

$$\left[[K_L]+\frac{1}{2}[K_{NL1}]+\frac{1}{3}[K_{NL2}]\right]\{\delta\}-\omega^2[M]\{\delta\}=0 \tag{22}$$

where ω is the nonlinear frequency. The frequency–amplitude relation is obtained by solving Eq. (22) through finite element procedure in conjunction with direct iteration technique.

The frequency–amplitude relation for the nonlinear free vibration problem is evaluated using the eigenvalue formulation. The nonlinear eigenvalue problem is solved employing an iterative procedure. The iteration starts from a corresponding normalized initial mode shape obtained from

linear analysis ($[K_{NL1}] = [K_{NL2}]=0$), with amplitude scaled up by a desired value. This initial mode shape is then used for evaluating the nonlinear stiffness matrices $[K_{NL1}]$ and $[K_{NL2}]$ given in Eq. (22). Then, the eigenvalue and its associated eigenvector are obtained using the standard eigenvalue extraction algorithm. This eigenvector is again normalized and scaled up by the same amplitude for updating the nonlinear stiffness matrices and the iteration continues until the frequency and the eigenvector evaluated from the subsequent two iterations are within the tolerance limit of 0.001%. Such iterative solution procedure is continued for different assumed amplitude of vibration.

In the present work, a C^1 continuous 3-noded beam element with four degrees of freedom at the end-nodes (u_0, w_0, $w_{0,x}$ & θ) and two at the internal node (u_0 & θ) is employed, as depicted in Fig. 2b. The transverse displacement function, w_0 is represented using Hermite shape functions whereas the in-plane displacement (u_0) and the cross-sectional rotation (θ) are assumed to be in the form of quadratic functions. If the original interpolation functions for the 3-noded element considered here are used directly to interpolate the field variables, u_0 and w_0, in deriving the membrane strains, the element will lock and show oscillation in the membrane stresses. Field consistency requires that the membrane strain $\varepsilon_0=u_0' + \frac{w_0}{R}$, *i.e.* the first two terms in the expression ε_{11} in Eq. (16b), must be interpolated in a consistent manner. Thus, we need substitute shape function for w_o to be consistent with $u_{0,x}$ in ε_0 as outlined in the work of Babu *et al.* [45]. This is achieved by using a field-redistributed substitute shape function to interpolate those specific terms that must be consistent. For instance, one can choose the required substitute shape function for w_o to be least square approximation of original interpolation over the element domain. However, the shear strain γ_{13} in Eq. (16b) is interpolated consistently by the original shape functions for field variables θ, $w_{0,x}$ and u_0. The element is free from shear locking phenomenon. The element thus constructed is found free from shear and membrane locking, and poor convergence syndrome. It performs very well for both thick and thin curved beam case. All the energy terms were numerically calculated adopting full integration.

4. Results & Discussion

The analysis here is focused on the large amplitude free vibration of fairly thick and thin functionally graded graphene platelets reinforced porous curved metal matrix beams. The present investigation considers three types of distribution for both the porosity in the metal foam matrix and the dispersion of GPLs through the thickness of the beam. The effective modulus and density of the nanocomposite are evaluated based on Halpin -Tsai model whereas the other material properties are evaluated by the rule of mixtures. The parametric study includes the effect of porosity, weight fraction of graphene platelets, distribution of porosity and graphene platelet reinforcements. The effect of beam slenderness ratio, curvature of beams and boundary condition on the amplitude-frequency relationship is also brought out. For curved beams, the included angle $\phi \in \{15^0, 30^0, 45^0, 60^0, 90^0, 120^0\}$ is varied covering shallow to deep beam cases. The length-to-radius of gyration of beam ratio, $L/r_g \in \{20, 50, 100\}$ assumes various values corresponding to thick and thin beams.

Boundary Conditions: The following boundary conditions have been employed for the purpose of this study:

- simply supported(H-H): $u_0 = w_0 = 0 \quad at\ x = 0, L$
- clamped-clamped (C-C): $u_0 = \theta = w_0 = {w_0}' = 0 \quad at\ x = 0, L$
- clamped-hinged (C-H): $u_0 = \theta = w_0 = w_0' = 0 \quad at\ x = 0\ ;\ u_0 = w_0 = 0\ at\ x = L$

The properties of GPLs and metal matrix are taken as:

- Material*:* Young's modulus, E_{gpl}=1.01 TPa; density, ρ_{gpl}= 1062.5 kg/m^3; Poisson's ratio, v_{gpl}=0.186
- Geometry*:* width, w_{gpl}=1.5 μm, length, l_{gpl}=2.5 μm, thickness, t_{gpl}=1.5 nm,
- Metal matrix: Copper based metal- Young's modulus E_m=130 GPa; density, ρ_m= 8960 kg/m^3; Poisson's ratio, v_m=0.34

All results presented here, unless mentioned otherwise, are in the non-dimensional form as mentioned below:

$$\Omega = \omega L^2 \sqrt{\frac{m}{E_m I}} \; ; \; where \; m = \rho h \; and \; I = h^3/12$$

Before proceeding for the detailed study, a convergence study is carried out by varying the element discretization as shown in Table 1 and it is observed from Table that 32 elements idealisation is found to be sufficient for the present analysis. Next, the present model is tested considering problems for which results are available in the literature. Considering the functionally graded GPL reinforced porous straight beams, the linear vibration analysis is made and the fundamental frequencies obtained are assessed with those available in Ref. [39] in Fig. 3 for different types of GPL distribution. They are in very good agreement. Next, the nonlinear formulation is tested against the available solutions for the non-linear vibrations of isotropic beams. The nonlinear frequency ratios evaluated are presented in Table 2 and are in close agreement with Ref. [11]. In the absence of results on the large amplitude-frequency relationship for graphene platelets reinforced curved beams, an exhaustive numerical experimentation considering all the combinations for porosity and GPL distribution patterns is conducted to select the appropriate distributions that yields high beam stiffness. These results are tabulated in Table 3 and 4 for hinged and clamped curved composite beams. It is opined from these Tables that the uniform distribution for the presence of both the porosity and GPL in the metal matrix curved beam appears to render high stiffness compared to those of other combinations and therefore, unless otherwise specified, this configuration is treated for further analyses.

The influence of the porosity content e_p on the nonlinear free vibration characteristics of curved GPL reinforced porous composite beams is brought out in Figs. 4-9 for the selected values of GPLs weight fraction w_{gpl} (0%, 0.25% and 0.75%), and for the chosen values of beam slenderness ratio (L/r_g=20, 50, 100) covering thin and fairly thick, and varying the beam included angle

representing shallow to deep cases ($\phi = 30^0$, 120^0). This investigation is shown for hinged-hinged case (Figs. 4-6) and clamped boundary condition (Figs.7-8) to understand effect of boundary conditions on the frequency-amplitude relationship. It is observed from these Figures that the increase in porosity content in the matrix results in decrease in the degree of hardening nonlinear behaviour of the beam. The rate of increase in frequency with amplitude is in general linear for the shallow curved beam whereas it is nonlinear and depends on the range of amplitude for the deep beam case. It is further seen that the inclusion of graphene platelets as reinforcements enhances the stiffness of the beam which in turn increases in nonlinear frequency values. For instance, in the case of thin (L/r_g=100, e_p=0) simply supported beams, while comparing beams with w_{gpl}= 0% and w_{gpl}= 0.75%, it can be observed that the addition of GPL results in 24% increase in frequency in the case of shallow beam (ϕ=30^o) and 28% increment for deep beams (ϕ=120^o) at the maximum amplitude of vibration considered here. For clamped beams of identical specification with the addition of GPL results in 25% increment for shallow beams and approximately 16% for deep curved case, thus resulting in increased hardening nonlinear behaviour. Furthermore, one can notice there is a sudden drop off in the nonlinear frequency at certain amplitude for moderately thick and thin shallow beams as highlighted in Figs. 4-5. The frequency then increases gradually with the increase in amplitude exhibiting hardening type of non-linear behaviour. The drop off in frequency shows a kind of instability and is possibly attributed to the change in stiffness properties and thus leading to the redistribution of mode shape, and also the participation of higher modes depending on the vibration amplitude and the value of geometrical parameter. This phenomenon of sudden decrease of non-linear stiffness are reported in the literature while investigating the postbuckling stability and strength of the plates subjected to thermal loadings [46-48], and recently on the nonlinear vibration of plates [49-51,15]. The sudden drop off in stiffness occurs at higher amplitude of vibration regardless of porosity level. However, for the range of amplitude considered here, the occurrence of such phenomenon is not appeared for deep curved beam case and the degree of hardening nonlinearity increases with the inclusion of GPLs. The effect of increase in the slenderness ratio of the beam is to decrease the degree of hardening nonlinear behaviour and the rate of change in the hardening behaviour is constant with amplitude. Similar study

is presented for clamped case in Figs. 7-8 for two values of L/r_g equal to 20 and 100. It is evident from these figures that the clamped beams show higher non-dimensional frequency compared to those of hinged cases, as expected. The nonlinear vibration behaviour is however qualitatively same as that of hinged-hinged case.

Figs. 9-10 depict the effect of weight fraction of GPL on the large amplitude free vibration of hinged/clamped shallow and deep curved beams ($\phi = 15^0, 45^0, 90^0$) with L/r_g = 20, 50, 100. It is inferred that the hardening behaviour increase with the increase in weight fraction of GPLs. Furthermore, it is noticed from these Figures that the phenomenon of dropping off frequency is in general more prevalent for thicker beams. However, it is also dependent to some extent on the slenderness ratio and the beam included angle. It is further shown that the increase in curvature of the beam shift the occurrence of frequency drop off phenomenon to lower w/r_g ratio especially for thick beam case as brought out in Fig.9 (a) and Fig. 10 (a). This can be attributed to the increase in the membrane energy due to the curvature of the beam, thus affecting the amplitude-frequency relationship. It can be also opined that the value frequency ratio of nonlinear to linear vibration case is in general more for the shallow beam compared to those of deep case. The influence of slenderness ratio results in increasing the nonlinear frequency ratio. The numerical experimentation is also conducted for clamped-hinged beam and the results are shown in Table 5 by varying L/r_g equal to 20 and 50 and w/r_g value up to 3. The behaviour of hinged-clamped beam is qualitatively very similar to that hinged or clamped case. However, it requires more elements for achieving converged solutions.

The normalized mode shapes corresponding to the first fundamental modes are presented in Fig. 11 for different boundary conditions for the selected beam cases. It is viewed from this Figure that the amplitude of inward travelling mode is more than that of outward deflection and this is due to the presence of curvature in the beam. It is also further that the fundamental mode can be either symmetric or antisymmetric depending on shallowness and slenderness ratio of the curved beam. Fig. 12 describes the mode shapes including the redistribution of modes happening at certain amplitudes of vibration which are responsible for the sudden drop off in frequencies of the beams. Lastly, the influence of geometry of GPL on the nonlinear frequency against amplitude is depicted in Fig. 13

considering a hinged-hinged curved beam (L/r_g =50, e_p= 0.5; w_{gpl} = 1%; ϕ=60^0). It is opined from this Figure that the increase in thickness and aspect ratios of GPL decreases the degree hardening effect whereas the aspect ratio does not change the nonlinear vibration characteristics of beam.

5. Conclusion

The application of finite element approach coupled with higher-order SIN model is introduced for predicting the large amplitude free vibration behavior of graphene platelets reinforced porous curved composite beams. The performance of the numerical model is compared with the available results in the literature. A comprehensive study is carried out to highlight the influence of various design parameters pertaining to the geometry and material slenderness ratio and boundary conditions, curvature of curved beam and the distribution pores and GPLs in the metal foam matrix of the beam on the nonlinear frequency parameter against the amplitudes of vibration curved beams. From the present analysis, some of the remarks made are as follows:

1. The GPL distribution patterns can affect the beam nonlinear frequency considerably in comparison with those of pores distribution pattern in the metal matrix.
2. The presence of porosity in the matrix decreases the degree of hardening nonlinear behavior whereas the inclusion of GPL enhanced the hardening characteristics of the curved beam.
3. The frequency-amplitude relation is more of linear for the shallow curved beam whereas it is in general nonlinear for deep beam up to certain range of amplitude.
4. Hardening trend increases for thick beam for the given amplitude ratio compared to the thin beam cases.
5. The frequency-amplitude relationship is highly nonlinear for deep curved beam case.
6. A sudden drop off in the nonlinear frequency is exhibited at certain amplitude for both thick and thin shallow beams depending on the level of porosity and the addition of GPLs.

7. The increase in the slenderness ratio of the beam decreases the degree of hardening nonlinear behaviour.
8. The first fundamental mode shape can be symmetric or antisymmetric depending on the slenderness ratio and deepness of the curved beam.
9. The maximum amplitude of mode shape pertaining to deep curved beam occurs in the inward direction compared to the outward deflection.
10. The clamped boundary condition shows higher non-dimensional frequency compared to those hinged case.
11. The aspect and thickness ratios affect the degree of hardening nonlinearity of the beam.
12. It may be worth in investigating the proposed problem for thick beam cases using higher-order model with the inclusion of thickness stretching effect.

References

[1]. Banhart J. Manufacture, characterisation and application of cellular metals and metal foams. Prog Mater Sci 2001;46:559–632. doi:https://doi.org/10.1016/S0079-6425(00)00002-5.

[2]. Qin J, Chen Q, Yang C, Huang Y. Research process on property and application of metal porous materials. J Alloys Compd 2016;654:39–44.

[3]. Ashby MF A, Evans A A, Fleck NA A, Gibson LJ A, Hutchinson JW A, Wadley HNG A, et al. Metal Foams: A Design Guide. Appl Mech Rev 2001;54:B105–6.

[4]. Lefebvre L-P, Banhart J, Dunand DC. Porous Metals and Metallic Foams: Current Status and Recent Developments. Adv Eng Mater 2008;10:775–87. doi:10.1002/adem.200800241.

[5]. Li Z, Young RJ, Wilson NR, Kinloch IA, Vallés C, Li Z. Effect of the orientation of graphene-based nanoplatelets upon the Young's modulus of nanocomposites. Compos Sci Technol 2016;123:125–33. doi:https://doi.org/10.1016/j.compscitech.2015.12.005.

[6]. Atif R, Shyha I, Inam F. Mechanical, Thermal, and Electrical Properties of Graphene-Epoxy Nanocomposites-A Review. Polymers (Basel) 2016;8:281. doi:10.3390/polym8080281.

[7]. Mittal G, Dhand V, Rhee KY, Park S-J, Lee WR. A review on carbon nanotubes and graphene as fillers in reinforced polymer nanocomposites. J Ind Eng Chem 2015;21:11–25. doi:https://doi.org/10.1016/j.jiec.2014.03.022.

[8]. Heyliger PR, Reddy JN. A higher order beam finite element for bending and vibration problems. J Sound Vib 1988;126:309–26. doi:https://doi.org/10.1016/0022-460X(88)90244-1..

[9]. Sarma BS, Varadan TK. Lagrange-type formulation for finite element analysis of non-linear beam vibrations. J Sound Vib 1983;86:61–70. doi:https://doi.org/10.1016/0022-460X(83)90943-4.

[10]. Sarma BS, Varadan TK. Ritz finite element approach to nonlinear vibrations of beams. Int J Numer Methods Eng 1984;20:353–67. doi:10.1002/nme.1620200213.

[11]. Sarma BS, Varadan TK. Certain discussions in the finite element formulation of nonlinear vibration analysis. Comput Struct 1982;15:643–6. doi:https://doi.org/10.1016/S0045-7949(82)80004-7.

[12]. Rao G V, Raju I S, Raju K. Nonlinear vibrations of beams considering shear deformation and rotary inertia. AIAA J 1976;14:685–7. doi:10.2514/3.7138.

[13]. Sathyamoorthy M. Recent Research in Nonlinear Analysis of Beams. Shock Vib Dig 1985;17:19–27. doi:10.1177/058310248501700905.

[14]. B.P. Patel, M. Ganapathi, M. Touratier, A STUDY ON NON-LINEAR FREE VIBRATION OF CANTILEVER BEAMS, J. Sound Vib. 207 (1997) 123–127. doi:https://doi.org/10.1006/jsvi.1997.1086.

[15]. A. Pagani, R. Augello, E. Carrera, Frequency and mode change in the large deflection and post-buckling of compact and thin-walled beams, J. Sound Vib. 432 (2018) 88–104. doi:https://doi.org/10.1016/j.jsv.2018.06.024.

[16]. Kapania RK, Raciti S. Nonlinear vibrations of unsymmetrically laminated beams. AIAA J 1989;27:201–10. doi:10.2514/3.10082.

[17]. Iu VP, Cheung YK, Lau SL. Non-linear vibration analysis of multilayer beams by incremental finite elements, Part I: Theory and numerical formulation. J Sound Vib 1985;100:359–72. doi:https://doi.org/10.1016/0022-460X(85)90292-5.

[18]. Singh G, Rao G V, Iyengar NGR. Analysis of the nonlinear vibrations of unsymmetrically laminated composite beams. AIAA J 1991;29:1727–35. doi:10.2514/3.10796.

[19]. Bassiouni AS, Gad-Elrab RM, Elmahdy TH. Dynamic analysis for laminated composite beams. Compos Struct 1999;44:81–7. doi:https://doi.org/10.1016/S0263-8223(98)00057-9.

[20]. Hajianmaleki M, Qatu MS. Vibrations of straight and curved composite beams: A review. Compos Struct 2013;100:218–32. doi:https://doi.org/10.1016/j.compstruct.2013.01.001.

[21]. Ke L-L, Yang J, Kitipornchai S. An analytical study on the nonlinear vibration of functionally graded beams. Meccanica 2010;45:743–52. doi:10.1007/s11012-009-9276-1.

[22]. Kitipornchai S, Ke LL, Yang J, Xiang Y. Nonlinear vibration of edge cracked functionally graded Timoshenko beams. J Sound Vib 2009;324:962–82. doi:https://doi.org/10.1016/j.jsv.2009.02.023.

[23]. Wu HL, Yang J, Kitipornchai S. Nonlinear vibration of functionally graded carbon nanotube-reinforced composite beams with geometric imperfections. Compos Part B Eng 2016;90:86–96. doi:https://doi.org/10.1016/j.compositesb.2015.12.007.

[24]. Feng C, Kitipornchai S, Yang J. Nonlinear free vibration of functionally graded polymer composite beams reinforced with graphene nanoplatelets (GPLs). Eng Struct 2017;140:110–9. doi:https://doi.org/10.1016/j.engstruct.2017.02.052.

[25]. Prathap G, Pandalai KA V. On asymptotic solutions to the non-linear vibrations of curved elements. J Sound Vib 1978;58:463–6. doi:https://doi.org/10.1016/S0022-460X(78)80053-4.

[26]. Reddy JN, Singh IR. Large deflections and large-amplitude free vibrations of straight and curved beams. Int J Numer Methods Eng 1981;17:829–52. doi:10.1002/nme.1620170603.

[27]. Noor AK, Knight NF. Nonlinear dynamic analysis of curved beams. Comput Methods Appl Mech Eng 1980;23:225–51. doi:https://doi.org/10.1016/0045-7825(80)90095-X.

[28]. Patel BP, Ganapathi M, Touratier M. Nonlinear free flexural vibrations/post-buckling analysis of laminated orthotropic beams/columns on a two parameter elastic foundation. Compos Struct 1999;46:189–96. doi:https://doi.org/10.1016/S0263-8223(99)00054-9.

[29]. Ganapathi M, Patel BP, Saravanan J, Touratier M. Application of spline element for large-amplitude free vibrations of laminated orthotropic straight/curved beams. Compos Part B Eng 1998;29:1–8. doi:https://doi.org/10.1016/S1359-8368(97)00025-5.

[30]. Hajianmaleki M, Qatu MS. Static and vibration analyses of thick, generally laminated deep curved beams with different boundary conditions. Compos Part B Eng 2012;43:1767–75. doi:https://doi.org/10.1016/j.compositesb.2012.01.019.

[31]. Touratier M. An efficient standard plate theory. Int J Eng Sci 1991;29:901–16. doi:https://doi.org/10.1016/0020-7225(91)90165-Y.

[32]. Ganapathi M, Patel BP, Boisse P, Polit O. Flexural loss factors of sandwich and laminated composite beams using linear and nonlinear dynamic analysis. Compos Part B Eng 1999;30:245–56. doi:https://doi.org/10.1016/S1359-8368(98)00063-8.

[33]. Liu F, Ming P, Li J. Ab initio calculation of ideal strength and phonon instability of graphene under tension. Phys Rev B 2007;76:64120. doi:10.1103/PhysRevB.76.064120.

[34]. Polit O, Anant C, Anirudh B, Ganapathi M. Functionally graded graphene reinforced porous nanocomposite curved beams: Bending and elastic stability using a higher-order model with thickness stretch effect. Compos Part B Eng 2019; 166:310-27 doi:https://doi.org/10.1016/j.compositesb.2018.11.074

[35]. Shokrieh MM, Esmkhani M, Shokrieh Z, Zhao Z. Stiffness prediction of graphene nanoplatelet/epoxy nanocomposites by a combined molecular dynamics–micromechanics method. Comput Mater Sci 2014;92:444–50. doi:https://doi.org/10.1016/j.commatsci.2014.06.002.

[36]. Affdl JCH, Kardos JL. The Halpin-Tsai equations: A review. Polym Eng Sci 1976;16:344–52. doi:10.1002/pen.760160512.

[37]. Rafiee MA, Rafiee J, Wang Z, Song H, Yu Z-Z, Koratkar N. Enhanced Mechanical Properties of Nanocomposites at Low Graphene Content. ACS Nano 2009;3:3884–90. doi:10.1021/nn9010472.

[38]. de Villoria RG, Miravete A. Mechanical model to evaluate the effect of the dispersion in nanocomposites. Acta Mater 2007;55:3025–31. doi:https://doi.org/10.1016/j.actamat.2007.01.007.

[39]. Chen D, Yang J, Kitipornchai S. Elastic buckling and static bending of shear deformable functionally graded porous beam. Compos Struct 2015;133:54–61. doi:https://doi.org/10.1016/j.compstruct.2015.07.052.

[40]. Kitipornchai S, Chen D, Yang J. Free vibration and elastic buckling of functionally graded porous beams reinforced by graphene platelets. Mater Des 2017;116:656–65. doi:https://doi.org/10.1016/j.matdes.2016.12.061.

[41]. Dong YH, Li YH, Chen D, Yang J. Vibration characteristics of functionally graded graphene reinforced porous nanocomposite cylindrical shells with spinning motion. Compos Part B Eng 2018;145:1–13. doi:https://doi.org/10.1016/j.compositesb.2018.03.009.

[42]. Roberts AP, Garboczi EJ. Elastic moduli of model random three-dimensional closed-cell cellular solids. Acta Mater 2001;49:189–97. doi:https://doi.org/10.1016/S1359-6454(00)00314-1.

[43]. Roberts AP, Garboczi EJ. Computation of the linear elastic properties of random porous materials with a wide variety of microstructure. Proc R Soc London Ser A Math Phys Eng Sci 2002;458:1033–54. doi:10.1098/rspa.2001.0900.

[44]. Polit O, Merzouki T, Ganapathi M. Elastic stability of curved nanobeam based on higher-order shear deformation theory and nonlocal analysis by finite element approach. Finite Elem Anal Des 2018;146:1–15. doi:https://doi.org/10.1016/j.finel.2018.04.002.

[45]. C.R. Babu, G. Prathap, A linear thick curved beam element, Int. J. Numer. Methods Eng. 23 (1986) 1313–1328. doi:10.1002/nme.1620230709.

[46]. G. Singh, G.V. Rao, N.G.R. Iyengar, Thermal postbuckling behavior of laminated composite plates, AIAA J. 32 (1994) 1336–1338. doi:10.2514/3.12143.

[47]. M. Ganapathi, M. Touratier, A study on thermal postbuckling behaviour of laminated composite plates using a shear-flexible finite element, Finite Elem. Anal. Des. 28 (1997) 115–135. doi:https://doi.org/10.1016/S0168-874X(97)81955-5.

[48]. M.K. Singha, L.S. Ramachandra, J.N. Bandyopadhyay, Thermal postbuckling analysis of laminated composite plates, Compos. Struct. 54 (2001) 453–458. doi:https://doi.org/10.1016/S0263-8223(01)00117-9.

[49]. M.K. Singha, M. Ganapathi, Large amplitude free flexural vibrations of laminated composite skew plates, Int. J. Non. Linear. Mech. 39 (2004) 1709–1720. doi:https://doi.org/10.1016/j.ijnonlinmec.2004.04.003.

[50]. N. Sundararajan, T. Prakash, M. Ganapathi, Nonlinear free flexural vibrations of functionally graded rectangular and skew plates under thermal environments, Finite Elem. Anal. Des. 42 (2005) 152–168. doi:https://doi.org/10.1016/j.finel.2005.06.001.

[51]. M. Talha, B.N. Singh, Large amplitude free flexural vibration analysis of shear deformable FGM plates using nonlinear finite element method, Finite Elem. Anal. Des. 47 (2011) 394–401. doi:https://doi.org/10.1016/j.finel.2010.11.006.

Legends for Figures

Figure 1. Distribution of porosity and GPLs in the thickness direction: (a) Porosity; (b) GPLs.

Figure 2. a) Geometrical parameters of curved beam; b) Beam element with the degrees of freedom.

Figure 3. Comparison of fundamental frequency increment of GPL reinforced straight beam with different GPL distributions (e_p=0.5, L/h=20, Symmetric porosity distribution).

Figure 4. The amplitude-frequency relation with different levels of porosity (e_p) for hinged-hinged GPL curved beams with L/r_g=20: a) w_{gpl} =0.0% ; b) w_{gpl} =0.25% ; c) w_{gpl} =0.75%.

Figure 5. The amplitude-frequency relation with different levels porosity (e_p) for hinged-hinged curved beams with L/r_g =50: a) w_{gpl} =0.0% ; b) w_{gpl} =0.25% ; c) w_{gpl} =0.75%.

Figure 6. The amplitude-frequency relation with different levels porosity (e_p) for hinged-hinged curved beams with L/r_g =100: a) w_{gpl} =0.0%; b) w_{gpl} =0.25%; c) w_{gpl} =0.75%.

Figure 7. The amplitude-frequency relation with different levels porosity (e_p) for clamped-clamped curved beams with L/r_g =20: a) w_{gpl} =0.0%; b) w_{gpl} =0.25% ; c) w_{gpl} =0.75%.

Figure 8. The amplitude-frequency relation with different levels porosity (e_p) for clamped-clamped curved beams with L/r_g =100: a) w_{gpl} =0.0%; b) w_{gpl} =0.25%; c) w_{gpl} =0.75%.

Figure 9: The amplitude-frequency relation with different levels of GPL weight fraction for hinged-hinged curved beams with e_p=0.5: a) L/r_g = 20; b) L/r_g = 50; c) L/r_g = 100.

Figure 10: The amplitude-frequency relation with different levels of GPL weight fraction for clamped-clamped curved beams with e_p=0.5: a) L/ρ = 20; b) L/ρ = 50; c) L/r_g = 100.

Figure 11: Normalized mode shapes at the mid-plane of straight and curved beams with ampllitudes (L/r_g =50 for e_p=0.5 and w_{gpl} =1%) a) Clamped-Clamped; b) Clamped-Hinged; c) Hinged-Hinged.

Figure 12: Redistribution of mode shapes with amplitude around instability zone (L/r_g = 20, e_p = 0.5 and ϕ= 90^o) for clamped-clamped composite curved beams.

Figure 13: The amplitude-frequency relation for different values of GPL geometry, $(l/w)_{gpl}$ & $(l/t)_{gpl}$ (e_p = 0.5;

L/r_g =50, w_{gpl}=1%, ϕ=60^o, symmetric distribution type for Porosity and GPLs).

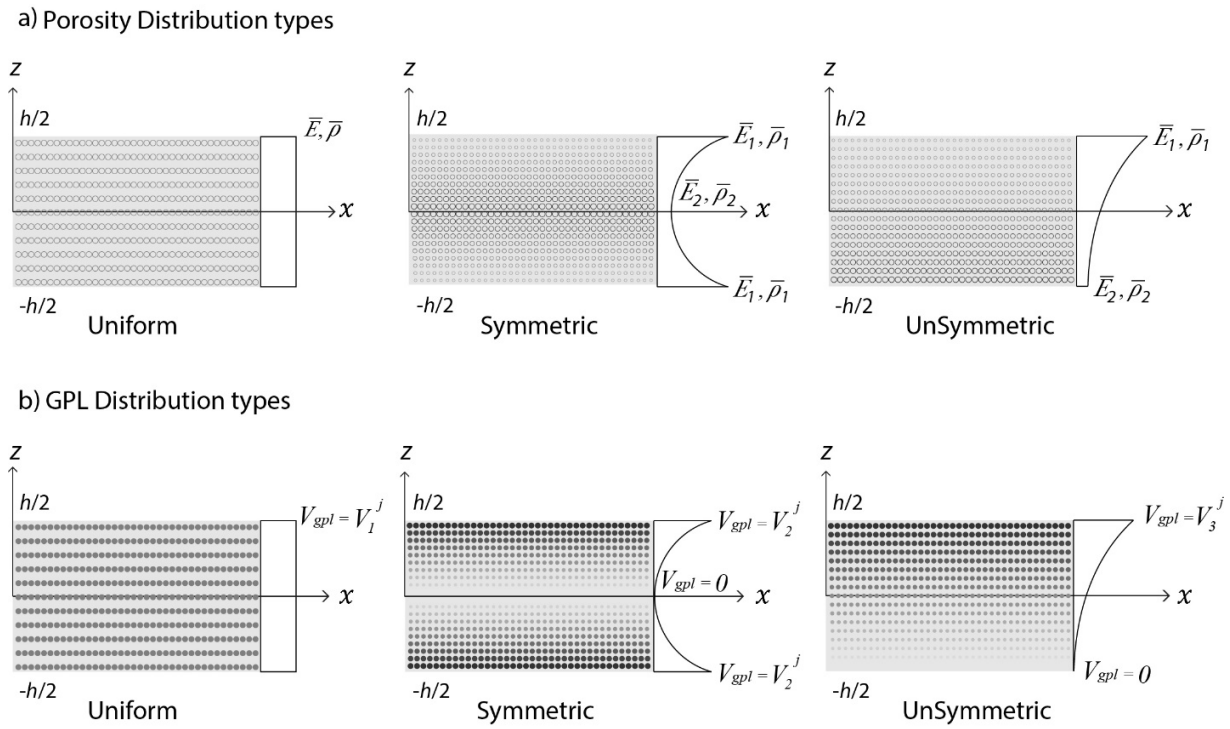

Figure 1. Distribution of porosity and GPLs in the thickness direction: (a)Porosity; (b) GPLs.

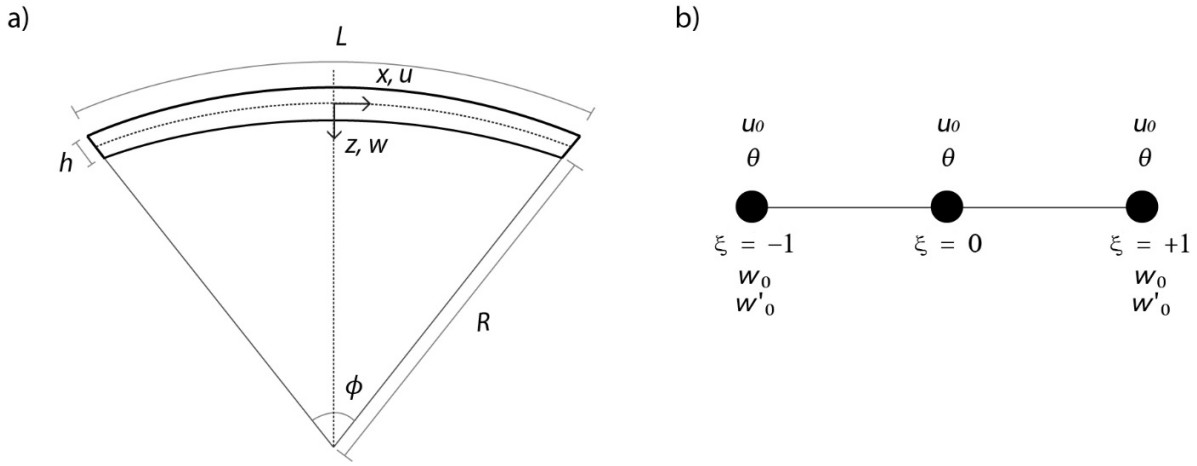

Figure 2. a) Geometrical parameters of curved beam; b) Beam element with the degrees of freedom.

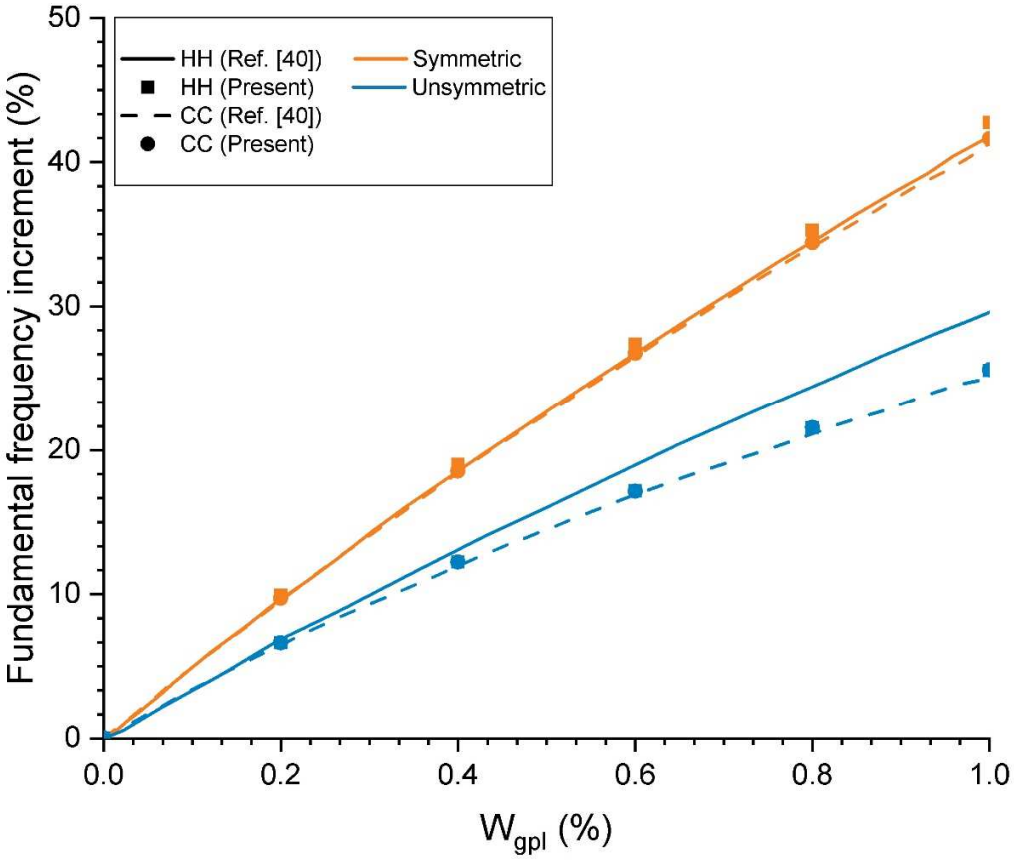

Figure 3. Comparison of fundamental frequency increment of GPL reinforced straight beam with different GPL distributions (e_p=0.5, L/h=20, Symmetric porosity distribution).

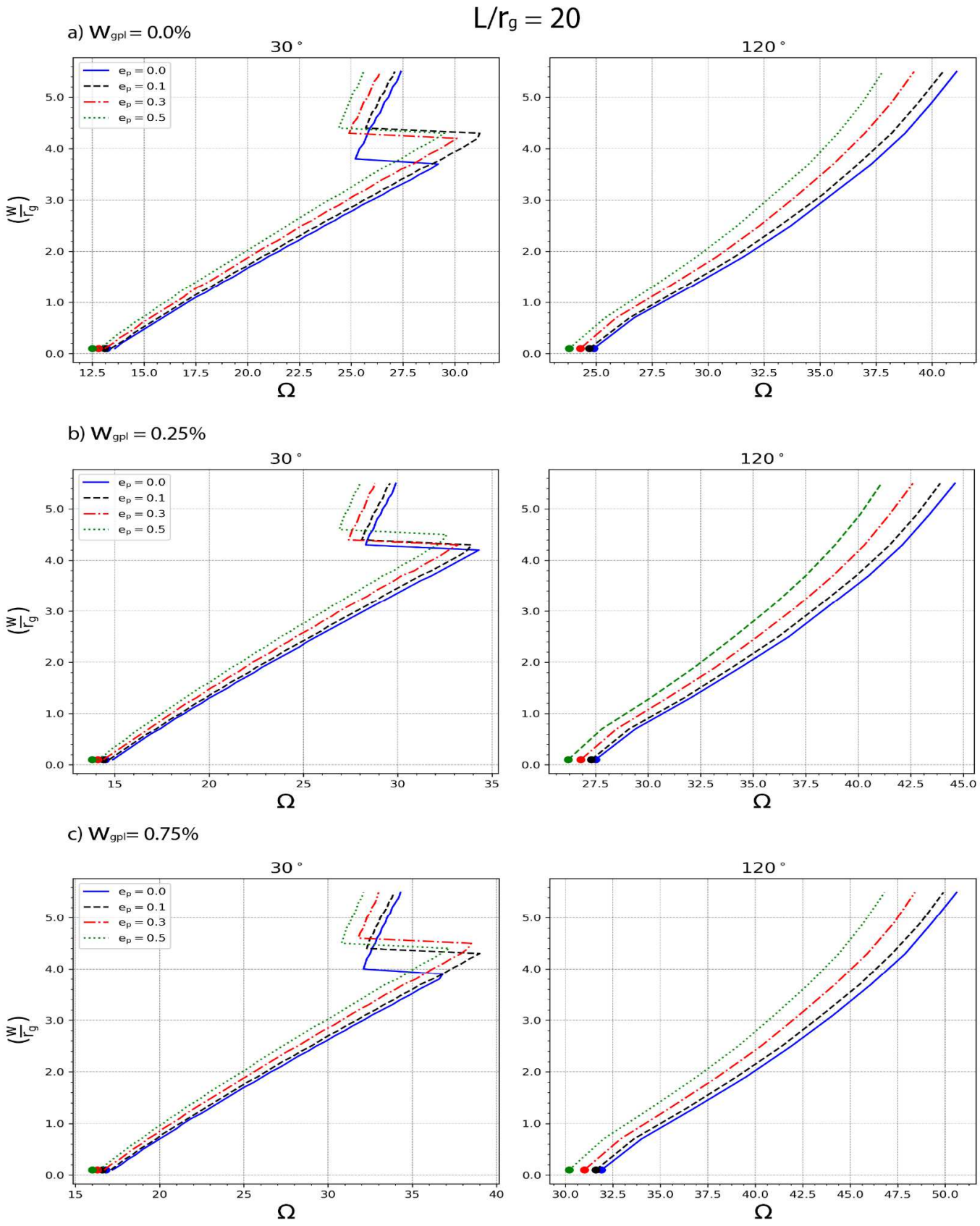

Figure 4. The amplitude-frequency relation with different levels of porosity (e_p) for hinged-hinged GPL curved beams with L/r_g=20: a) w_{gpl} =0.0% ; b) w_{gpl} =0.25% ; c) w_{gpl} =0.75%.

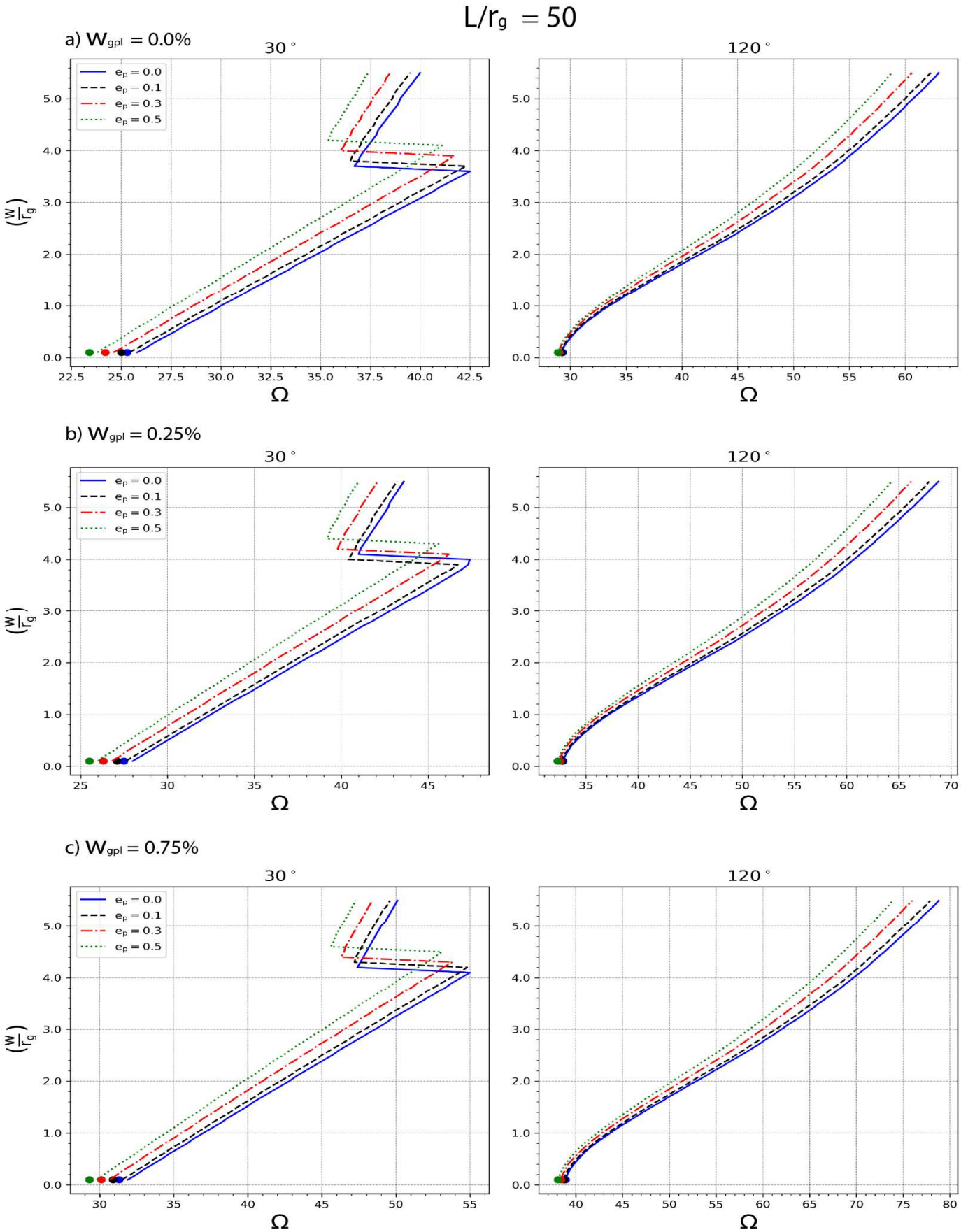

Figure 5. The amplitude-frequency relation with different levels porosity (e_p) for hinged-hinged curved beams with L/r_g =50: a) w_{gpl} =0.0% ; b) w_{gpl} =0.25% ; c) w_{gpl} =0.75%.

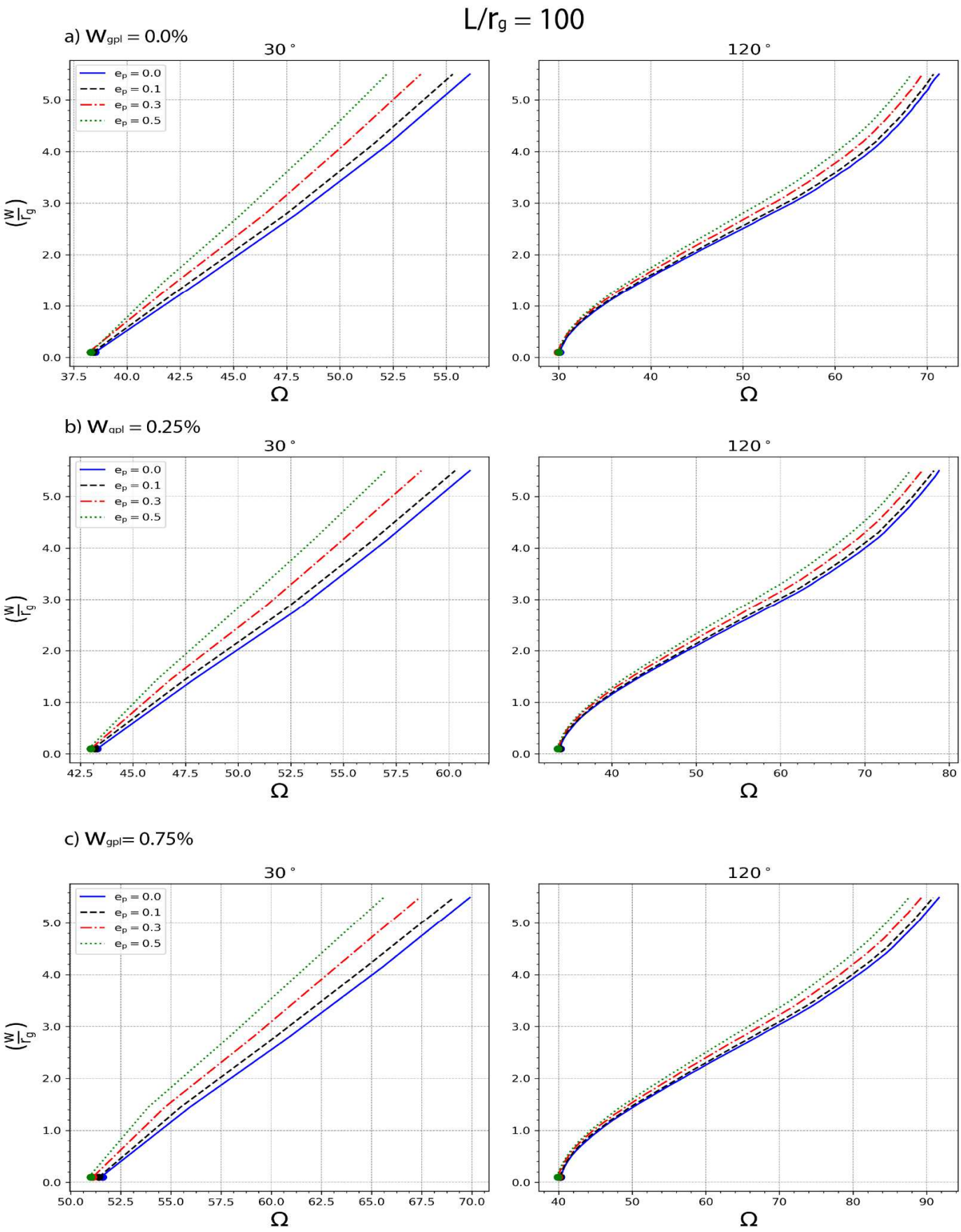

Figure 6. The amplitude-frequency relation with different levels porosity (e_p) for hinged-hinged curved beams with L/r_g =100: a) w_{gpl} =0.0% , b) w_{gpl} =0.25% c) w_{gpl} =0.75%.

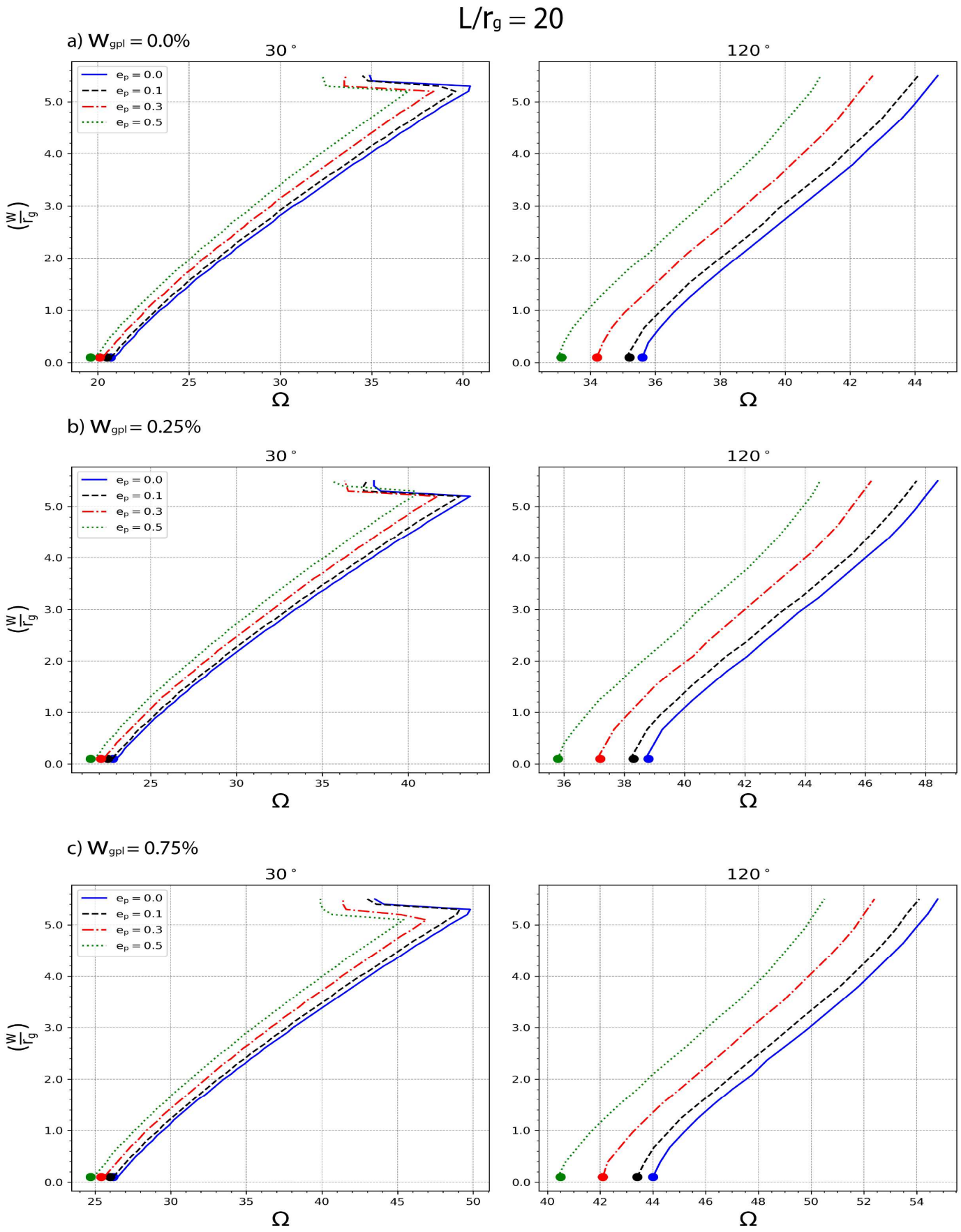

Figure 7. The amplitude-frequency relation with different levels porosity (e_p) for clamped-clamped curved beams with L/r_g =20: a) w_{gpl} =0.0%; b) w_{gpl} =0.25% ; c) w_{gpl} =0.75%.

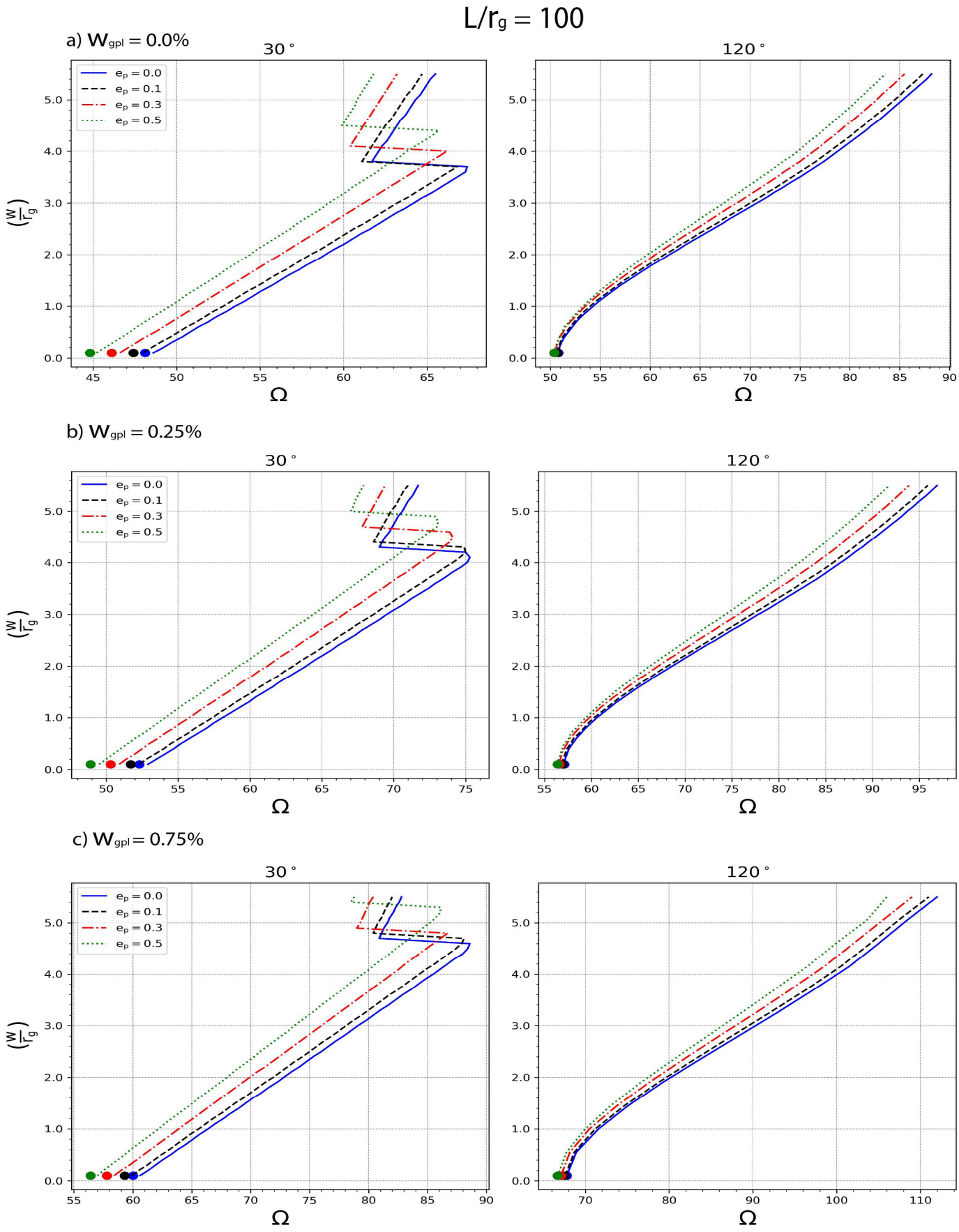

Figure 8. The amplitude-frequency relation with different levels porosity (e_p) for clamped-clamped curved beams with L/r_g =100: a) w_{gpl} =0.0%; b) w_{gpl} =0.25%; c) w_{gpl} =0.75%.

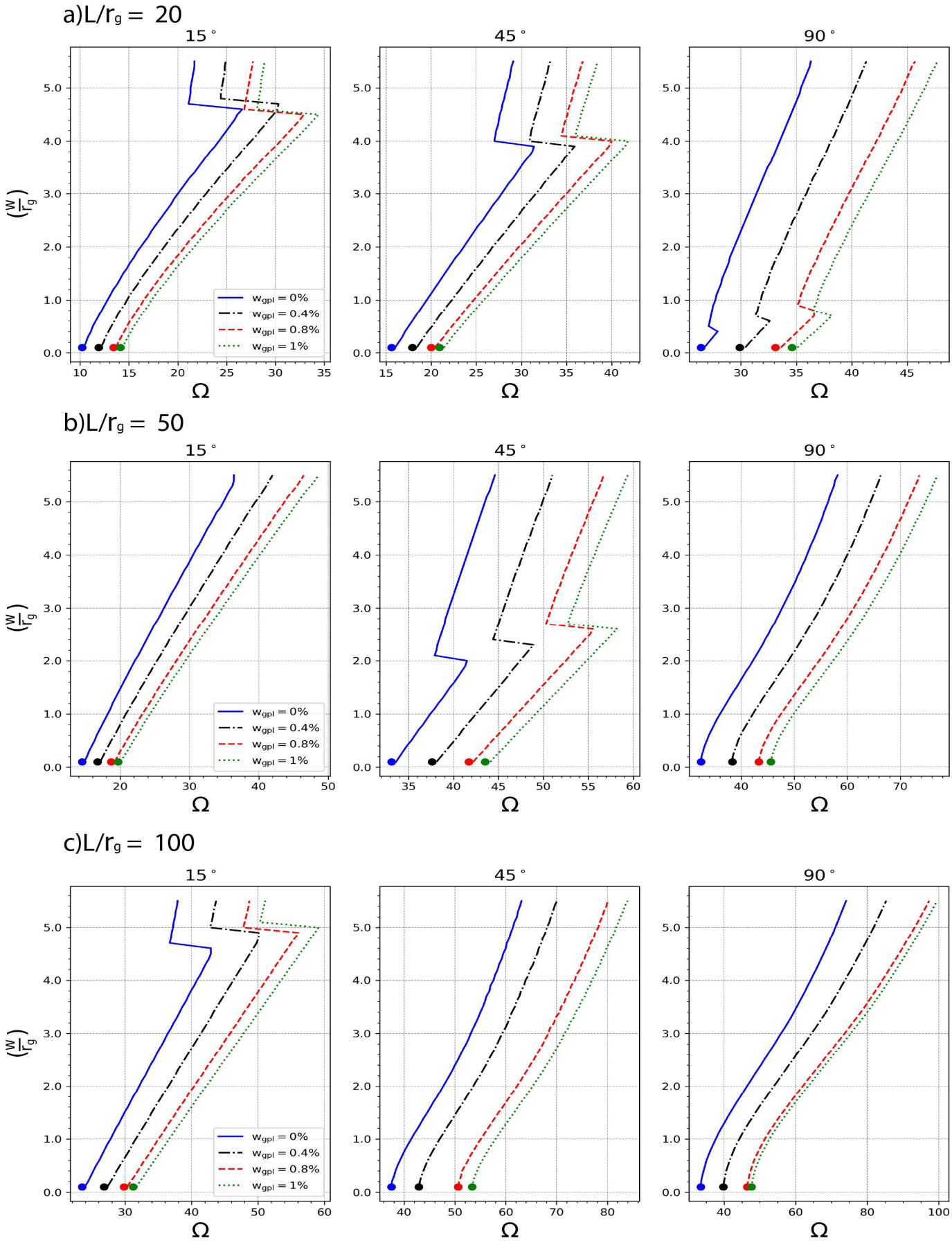

Figure 9: The amplitude-frequency relation with different levels of GPL weight fraction for hinged-hinged curved beams with e_p=0.5: a) L/r_g = 20; b) L/r_g = 50; c) L/r_g = 100.

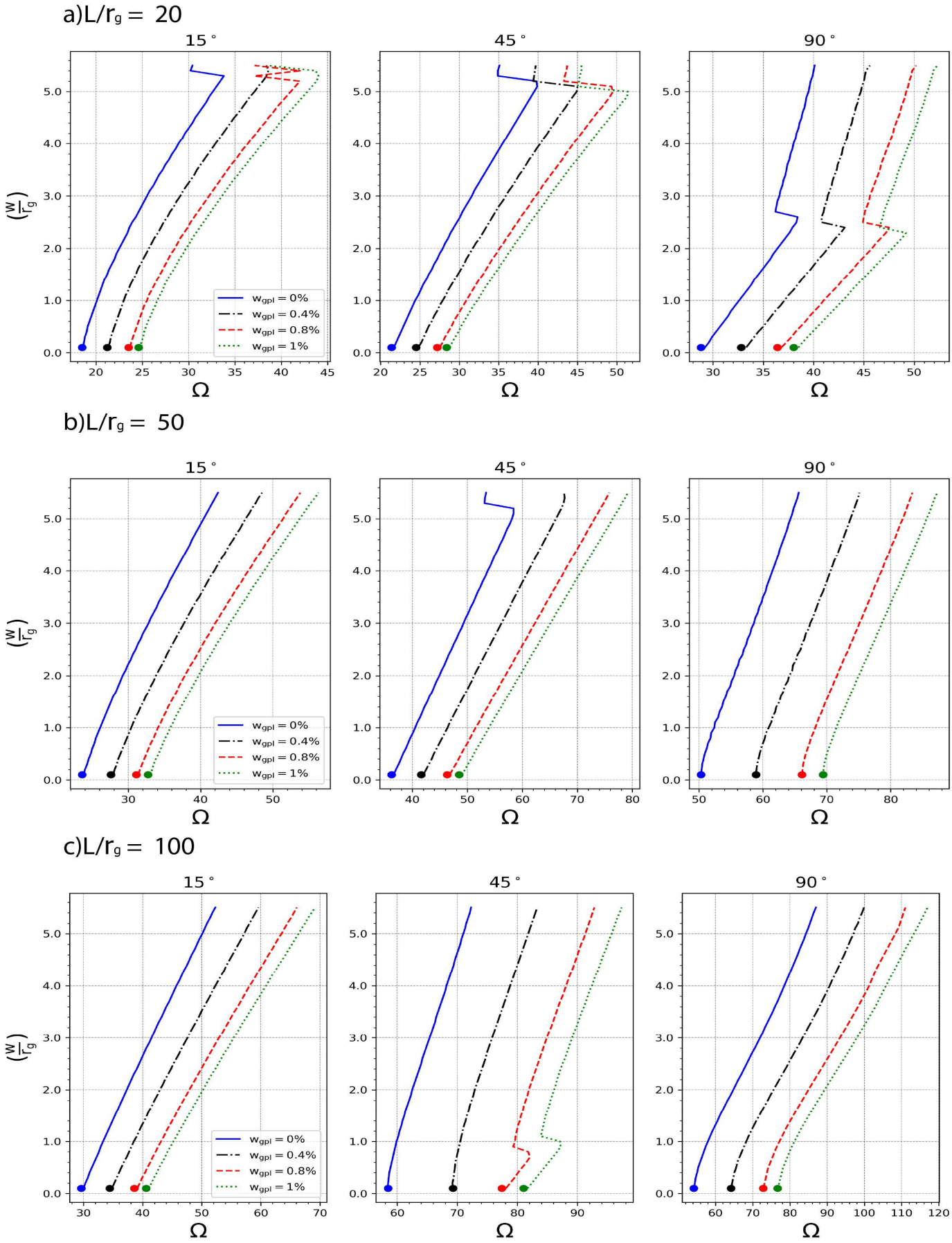

Figure 10: The amplitude-frequency relation with different levels of GPL weight fraction for clamped-clamped curved beams with e_p=0.5: a) L/ρ = 20; b) L/ρ = 50; c) L/r_g = 100.

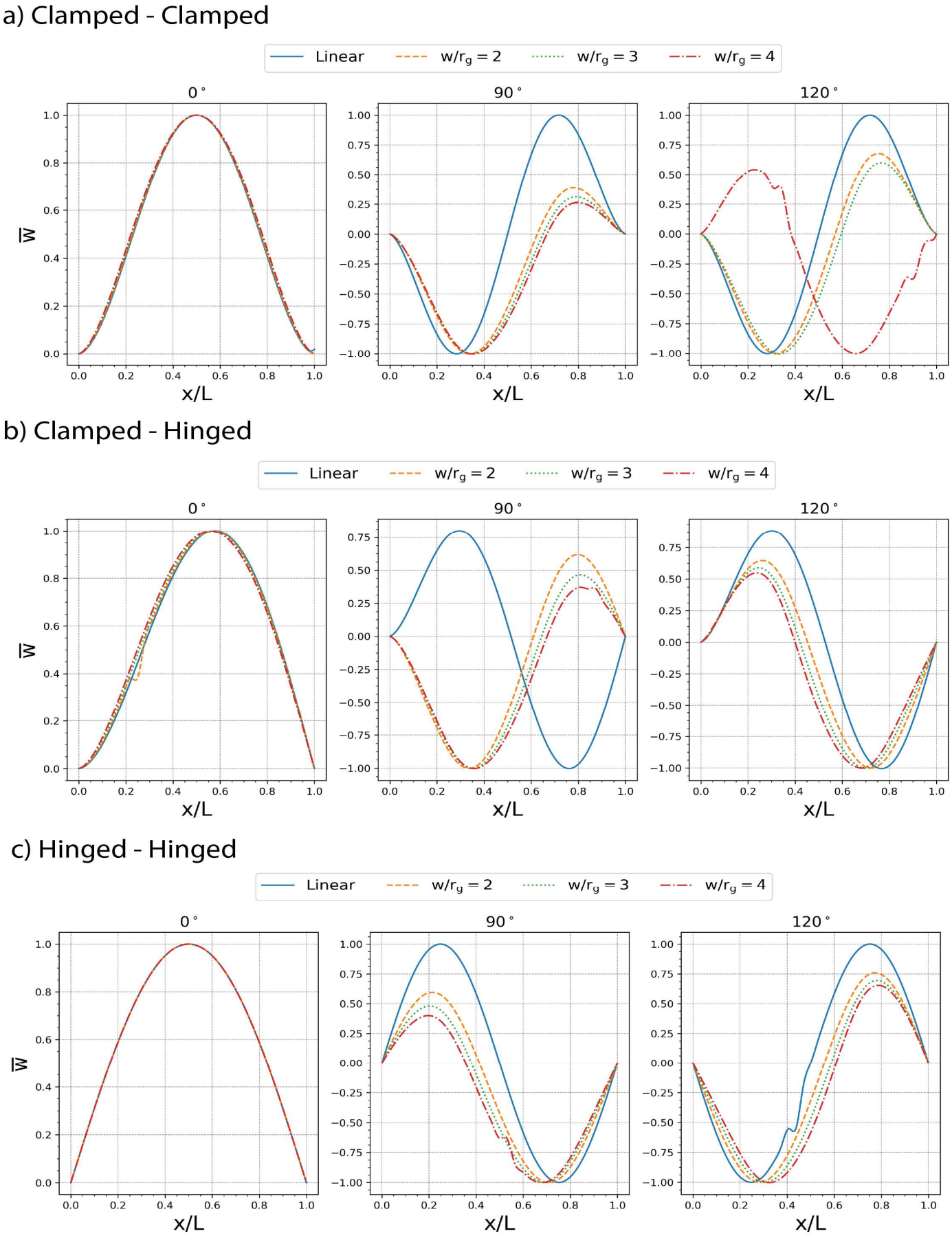

Figure 11: Normalized mode shapes at the mid-plane of straight and curved beams with amplitudes (L/r_g =50 for e_p=0.5 and w_{gpl} =1%) a) Clamped-Clamped; b) Clamped-Hinged; c) Hinged-Hinged.

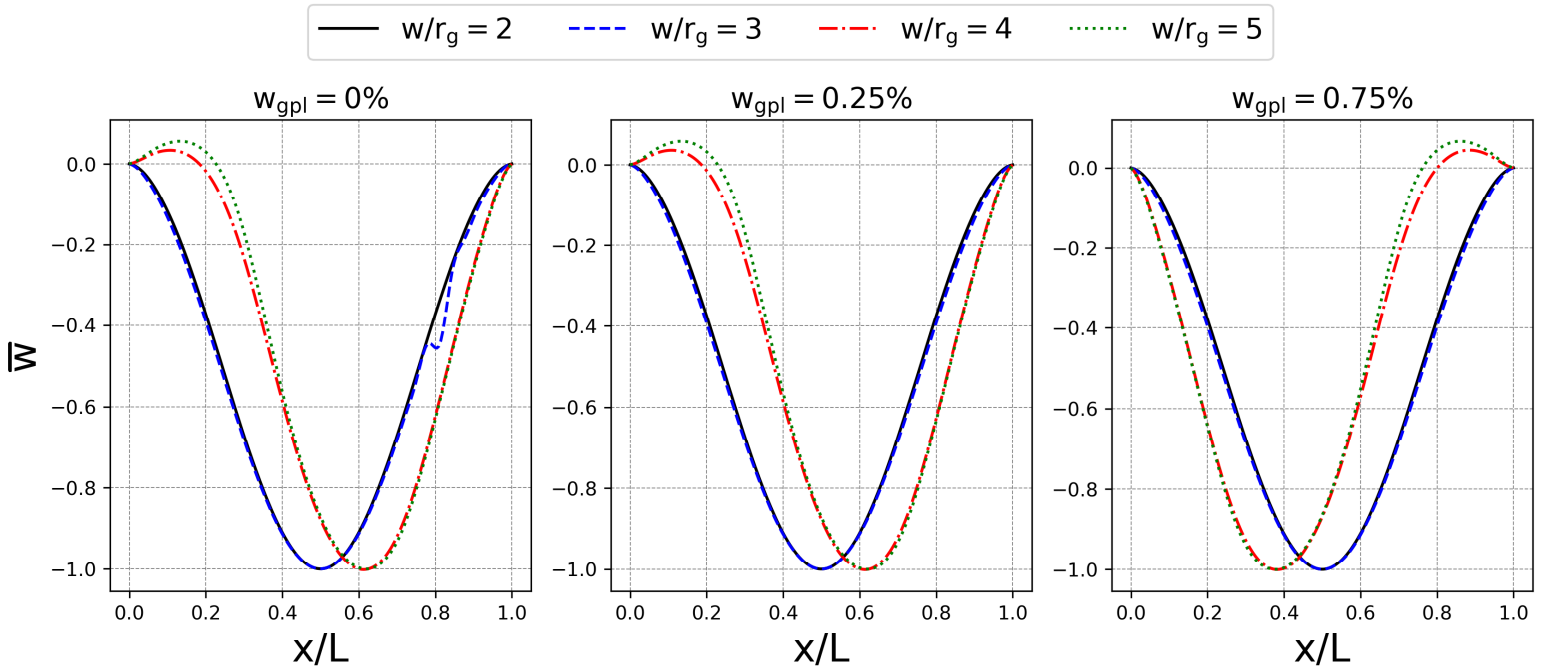

Figure 12: Redistribution of mode shapes with amplitude around instability zone (L/r_g = 20, e_p = 0.5 and ϕ= 90°) for clamped-clamped composite curved beams.

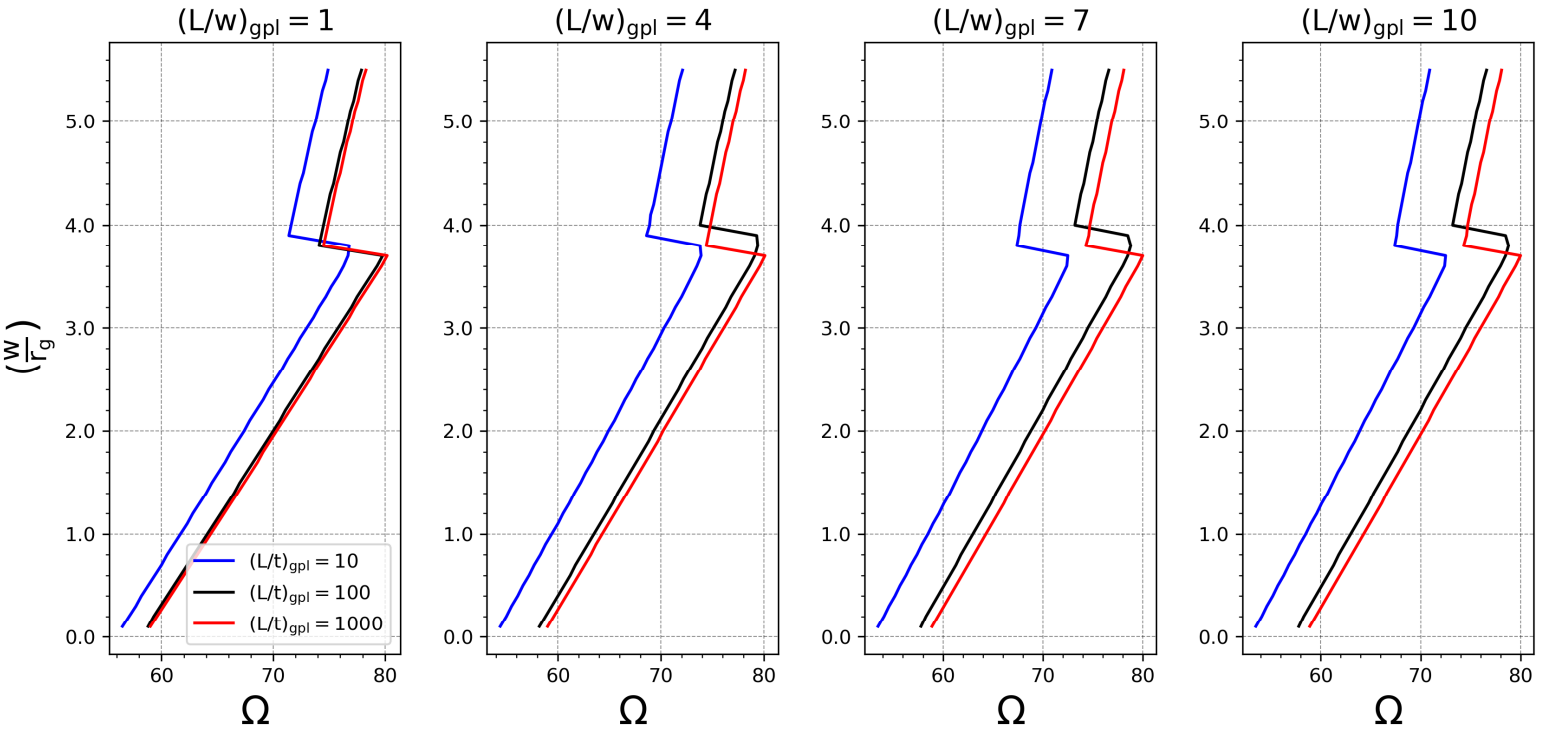

Figure 13: The amplitude-frequency relation for different values of GPL geometry, $(l/w)_{gpl}$ & $(l/t)_{gpl}$ (e_p = 0.5; L/r_g =50, w_{gpl}=1%, ϕ=60°, symmetric distribution type for Porosity and GPLs).

Legends for Tables

Table 1: Mesh convergence study for free vibration of porous composite curved beam (ϕ = 90º, e_p= 0.5, w_{gpl} = 1% - symmetric distribution for porosity and GPLs).

Table 2: Comparison of nonlinear frequency ratio for hinged-hinged isotropic straight beams with Ref. [11].

Table 3: Non-dimensional nonlinear frequency (Ω) against amplitude (w/r_g) for hinged-hinged curved beams with different types of GPL distribution and constant porosity value (e_p=0.5).

Table 4: Non-dimensional nonlinear frequency (Ω) against amplitude (w/r_g) for clamped-clamped curved beams with different types of GPL distribution and constant porosity value (e_p=0.5).

Table 5: Non-dimensional nonlinear frequency (Ω) against amplitude (w/r_g) for clamped-hinged curved beams with different types of porosity and GPL distribution.

Table 1: Mesh convergence study for free vibration of porous composite curved beam ($\phi = 90^o$, $e_p = 0.5$, $w_{gpl} = 1\%$ - symmetric distribution for porosity and GPLs).

L/r_g	Number of Element	Non-dimensional frequency (Ω) = $\omega L^2 \sqrt{\frac{m}{E_m h^2}}$			
		Hinged-Hinged		Clamped-Clamped	
		Formulation			
		Original	Consistent	Original	Consistent
20	**8**	34.618	34.617	37.979	37.976
	16	34.615	34.615	37.973	37.972
	32	34.615	34.615	37.972	37.972
	64	34.615	34.615	37.972	37.972
	128	34.615	34.615	37.972	37.972
50	**8**	45.652	45.614	69.870	69.818
	16	45.603	45.601	69.523	69.519
	32	45.600	45.600	69.414	69.414
	64	45.600	45.600	69.385	69.385
	128	45.600	45.600	69.380	69.380
100	**8**	47.873	47.720	77.085	76.875
	16	47.716	47.706	76.751	76.736
	32	47.706	47.705	76.692	76.691
	64	47.705	47.705	76.674	76.674
	128	47.705	47.705	76.657	76.669
1000	**8**	61.564	48.485	97.648	79.714
	16	49.443	48.470	81.121	79.661
	32	48.531	48.470	79.752	79.657
	64	48.473	48.469	79.663	79.657
	128	48.470	48.469	79.657	79.657
10000	**8**	329.436	48.493	416.415	79.744
	16	107.729	48.478	167.459	79.692
	32	54.317	48.477	88.623	79.689
	64	48.864	48.477	80.281	79.688
	128	48.477	48.477	79.726	79.688

Table 2: Comparison of nonlinear frequency ratio for hinged-hinged isotropic straight beams with Ref. [11].

w/r_g	$(\omega_{NL}/\omega_L)^2$	
	Ref.[11]	Present
0.2	1.0100	1.0114
0.4	1.0400	1.0405
0.6	1.0900	1.0910
0.8	1.1600	1.1618
1.0	1.2500	1.2528
2.0	2.0000	2.0101
3.0	3.2500	3.2688
4.0	5.0000	5.0306

Table 3: Non-dimensional nonlinear frequency (Ω) against amplitude (w/r_g) for hinged-hinged curved beams withdifferent types of GPL distribution and constant porosity value (e_p=0.5).

L/r_g	ϕ	Porosity Dist. Type	w/r_g=0			w/r_g=2			w/r_g=3			w/r_g=4		
			GPL Dist. Type			GPL Dist. Type			GPL Dist. Type			GPL Dist. Type		
			Sym.	Unsym.	Uniform	Sym.	Unsym.	Uniform	Sym.	Unsym.	Uniform	Sym.	Unsym.	Uniform
20	0°	Sym.	24.048	22.718	23.166	26.842	26.012	26.013	29.921	29.341	29.120	33.711	33.366	32.917
		UnSym.	23.128	21.339	21.988	26.327	24.923	25.254	29.602	28.463	28.623	33.570	32.710	32.675
		Uniform.	23.191	21.628	21.962	25.992	24.956	24.949	29.056	28.345	28.165	32.809	32.419	32.054
	30°	Sym.	26.088	24.617	25.189	33.055	31.903	32.167	37.475	36.396	36.569	42.272	41.219	41.325
		UnSym.	25.065	23.344	24.006	32.284	31.040	31.377	36.765	35.688	35.932	41.588	40.639	40.809
		Uniform.	25.196	23.591	24.050	32.095	30.963	31.223	36.454	35.496	35.697	41.171	40.342	40.502
	60°	Sym.	31.283	29.701	30.328	40.404	38.810	37.981	45.368	43.662	44.343	50.498	48.607	49.411
		UnSym.	30.181	28.713	29.249	39.307	38.109	38.537	44.201	43.032	43.493	49.212	47.992	48.554
		Uniform.	30.293	28.761	29.306	39.296	37.954	38.554	44.178	42.835	43.517	49.210	47.802	48.608
50	0°	Sym.	30.086	26.897	27.455	32.608	29.761	30.154	35.464	32.889	33.169	39.053	36.757	36.914
		UnSym.	27.764	24.339	25.194	30.539	27.548	28.189	33.590	30.982	31.450	37.380	35.162	35.446
		Uniform.	27.834	24.753	25.129	30.458	27.769	28.037	33.399	31.038	31.235	37.064	35.036	35.155
	30°	Sym.	39.467	36.746	37.210	49.054	46.701	47.039	54.235	52.017	52.298	59.557	57.451	57.674
		UnSym.	37.448	35.106	35.514	47.283	45.645	45.731	52.555	51.190	51.142	57.951	56.825	56.649
		Uniform.	37.385	35.038	35.395	47.048	45.217	45.531	52.233	50.601	50.896	57.538	56.079	56.353
	60°	Sym.	58.455	55.947	56.365	70.325	68.506	68.352	76.176	67.914	74.798	74.891	70.180	71.460
		UnSym.	56.577	55.061	55.077	68.486	62.368	67.305	74.326	64.816	66.057	71.484	67.542	68.581
		Uniform.	56.298	54.435	54.852	68.127	66.576	67.063	73.929	64.963	66.072	71.602	67.509	68.570

Table 4: Non-dimensional nonlinear frequency (Ω) against amplitude (w/r_g) for clamped-clamped curved beams with different types of GPL distribution and constant porosity value (e_p=0.5).

L/r_g	ϕ	Porosity Dist. Type	w/r_g=0			w/r_g=2			w/r_g=3			w/r_g=4		
			GPL Dist. Type			GPL Dist. Type			GPL Dist. Type			GPL Dist. Type		
			Sym.	Unsym.	Uniform	Sym.	Unsym.	Uniform	Sym.	Unsym.	Uniform	Sym.	Unsym.	Uniform
20	0°	Sym.	12.983	12.051	11.885	17.367	17.289	16.433	21.607	21.701	20.783	26.492	26.678	25.596
		UnSym.	12.282	11.508	11.135	17.323	17.350	16.399	21.688	21.920	20.911	26.630	26.867	25.854
		Uniform.	12.054	11.082	10.910	16.514	16.461	15.690	20.759	20.968	20.100	25.611	25.902	25.073
	30°	Sym.	16.986	17.959	16.049	26.321	27.168	25.464	31.569	32.314	30.696	36.306	32.172	36.197
		UnSym.	17.859	18.346	16.818	27.051	27.815	26.234	32.202	33.044	31.451	37.335	32.265	36.410
		Uniform.	16.135	17.033	15.299	25.440	26.360	24.886	30.628	31.529	30.151	36.089	30.932	35.654
	60°	Sym.	25.320	26.582	24.489	35.842	36.611	34.960	41.319	36.457	40.386	39.160	38.782	37.942
		UnSym.	26.490	27.071	25.626	36.604	33.403	35.865	36.873	35.839	35.678	39.155	38.186	38.029
		Uniform.	24.467	25.736	23.924	34.853	35.809	34.434	40.242	35.325	39.698	37.929	37.698	36.890
50	0°	Sym.	13.889	12.705	12.499	18.135	17.941	16.973	22.326	22.388	21.272	27.112	27.339	26.183
		UnSym.	12.981	12.026	11.602	18.002	17.942	16.877	22.393	22.566	21.421	27.326	27.629	26.521
		Uniform.	12.713	11.550	11.350	17.080	16.939	16.089	21.307	21.473	20.517	26.081	26.556	25.452
	30°	Sym.	30.990	32.496	30.002	41.995	43.168	40.954	47.615	48.665	46.529	53.288	46.683	52.145
		UnSym.	32.318	33.028	31.262	42.998	43.947	42.062	48.498	43.535	47.601	46.896	46.161	44.787
		Uniform.	29.930	31.422	29.357	40.781	42.115	40.327	46.309	47.606	45.898	51.882	44.680	43.147
	60°	Sym.	49.668	43.080	45.199	55.577	51.934	52.413	59.043	56.348	56.270	62.367	60.279	59.839
		UnSym.	44.885	38.532	40.810	52.922	49.194	50.376	57.293	54.251	55.008	61.063	58.653	58.925
		Uniform.	45.878	39.759	41.334	52.849	49.539	50.083	56.508	54.262	54.152	59.941	58.330	57.968

Table 5: Non-dimensional nonlinear frequency (Ω) against amplitude (w/r_g) for clamped-hinged curved beams with different types of porosity and GPL distribution.

L/r_g	ϕ	e_p	w/r_g=0			w/r_g=1			w/r_g=2			w/r_g=3		
			w_{gpl}(%)			w_{gpl}(%)			w_{gpl}(%)			w_{gpl}(%)		
			0	0.25	0.75	0	0.25	0.75	0	0.25	0.75	0	0.25	0.75
20	30°	0	16.405	18.087	20.973	19.817	21.690	24.953	23.777	25.899	29.635	28.100	30.226	34.611
		0.1	16.259	17.924	20.780	19.590	21.448	24.682	23.466	25.572	29.279	27.694	30.104	34.197
		0.3	15.958	17.584	20.370	19.470	21.315	24.108	22.814	24.886	28.526	26.874	29.224	33.428
		0.5	15.645	17.219	19.916	18.622	20.398	23.483	22.122	24.152	27.713	26.128	28.315	32.415
	120°	0	29.690	32.503	37.243	32.010	34.911	39.873	35.135	38.216	43.547	37.873	41.115	46.770
		0.1	29.376	32.141	36.808	31.625	34.484	39.379	34.676	37.719	42.986	37.352	40.557	46.150
		0.3	28.686	31.344	35.842	30.789	33.554	37.122	33.687	36.645	41.771	36.229	39.356	44.814
		0.5	27.878	30.403	34.694	28.910	32.486	37.050	32.576	35.432	40.390	34.982	38.015	43.315
50	30°	0	26.890	29.380	33.799	31.681	34.477	39.466	36.505	39.632	45.230	39.976	44.761	51.018
		0.1	26.562	29.041	33.437	31.254	34.038	39.001	35.985	39.098	44.665	39.647	44.152	50.362
		0.3	25.890	28.347	32.698	30.370	33.130	38.041	34.903	37.989	43.496	39.421	42.864	48.996
		0.5	25.214	27.648	31.950	29.459	32.196	37.054	33.774	36.834	42.281	38.105	41.507	47.566
	120°	0	37.990	42.474	50.103	41.721	46.334	54.254	48.622	53.484	61.928	55.079	60.600	69.735
		0.1	37.824	42.267	46.226	41.444	46.020	50.122	48.146	52.972	57.334	54.489	59.925	64.635
		0.3	37.527	41.876	49.280	40.909	45.398	52.584	47.177	51.917	59.975	53.426	58.521	67.428
		0.5	37.303	41.528	48.733	40.423	44.367	52.311	46.198	50.690	58.713	52.056	57.049	65.773